

Entangled Vortices: Onsager's geometrical picture of superfluid phase transitions

Adriaan M. J. Schakel[†]

Low Temperature Laboratory, Helsinki University of Technology, P.O. Box 2200, FIN-02015 HUT, Finland
(Dated: June 21, 2002)

Superfluid phase transitions are discussed from a geometrical perspective as envisaged by Onsager. The approach focuses on vortex loops which close to the critical temperature form a fluctuating vortex tangle. As the transition is approached, vortex lines proliferate and thereby disorder the superfluid state, so that the system reverts to the normal state. It is shown in detail that loop proliferation can be described in exactly the same way as cluster percolation. Picturing vortex loops as worldlines of bosons, with one of the spatial coordinates interpreted as the time coordinate, a quantitative description of vortex loops can be given. Applying a rotation (to superfluids) or a magnetic field (to superconductors), which suppresses the formation of vortex loops and instead can lead to open vortex lines along the field direction, is shown to be equivalent to taking the nonrelativistic limit. The nonrelativistic theory is the one often used to study vortex lattice melting and to describe the resulting entangled vortex liquid.

I. PREFACE

As classical fluids and gasses, superfluids, Bose-Einstein condensates, and also superconductors support vortices¹: extended line-like objects around which the fluid or gas executes a circular motion. In the classical world, vortices are better known as whirlpools (in fluids) and as whirlwinds (in the atmosphere) or also as tornadoes, or typhoons, depending on which side of the Pacific Ocean one lives. The velocity of the circular motion around a vortex line varies as the inverse of the distance to the rotation axis. The strong winds close to the center of a whirlwind or the so-called eye of a tornado are, incidentally, responsible for most of the damages caused by typhoons.

A striking difference with classical systems is that the circulation around these extended line objects in quantum systems is quantized. Given that a vortex usually is macroscopic in size and sets all the atoms or electrons of the system in motion, the quantization of circulation is truly remarkable and cannot in general be related to the quantization rules of quantum mechanics. Instead, as is well known, the quantization here is provided by topology².

The presence of vortices in superfluids and Bose-Einstein condensates is an emergent property, associated with the spontaneous breaking of global gauge symmetry³. In superconductors, this symmetry becomes a local one, which strictly speaking cannot be spontaneously broken, but the following argument is not affected by it. The vacuum manifold, defining the system's minimum of energy, is a circle S^1_{vac} parametrized by the phase of the spontaneously broken $U(1)$ gauge symmetry. If a vortex is circled once, the phase moves around the circle S^1_{vac} representing the vacuum manifold. A vortex therefore provides a map from the circle S^1_x in real space to S^1_{vac} . Such maps are

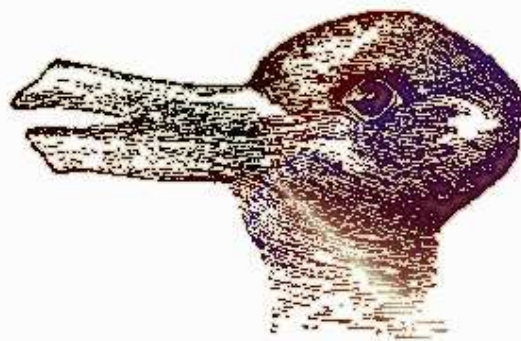


FIG. 1: Drawing, introduced by the psychologist J. Jastrow (1900), that depicts both a duck and a rabbit.

characterized by an integer winding number telling how often the map wraps around the circle S^1_{vac} when S^1_x in real space is circled once. The integer nature of the winding number explains the quantization of circulation around vortices in quantum systems. A vortex of a given winding number cannot be continuously deformed into one of a different winding number and hence is topologically stable.

In these lecture notes, superfluid phase transitions are discussed from the perspective of quantized vortices in the spirit of Onsager's picture of the transition in liquid ^4He ⁴. The description envisaged by Onsager is one entirely in terms of these one-dimensional objects, with their geometrical properties such as fractal dimension and configurational entropy. In the absence of an applied rotation (for superfluids) or magnetic field (for superconductors), vortices cannot terminate inside the system and must form closed loops. A superfluid phase transition is characterized in this picture by a fundamental change in the typical loop size. Whereas in the superfluid phase only finite loops are present, at the critical point infinite loops appear similar to the sudden appearance of a percolating cluster in percolation phenomena at criticality^{5,6,7,8}. In Feynman's words⁹: "The superfluid is pierced through and through with vortex line. We are describing the disorder of Helium I."

The similarity between vortex loop proliferation and cluster percolation is, as will be discussed, very close. It derives from a similarity in the cluster size and loop size distribution. Both have the same form containing two factors, one related to the entropy of a given cluster or loop configuration, and the other related to the Boltzmann weight assigned to the configuration. Close to criticality, both of these factors are parametrized by a single exponent. One specifies the algebraic behavior of the distribution at criticality, while the other describes how the Boltzmann factor tends to unity upon approaching the critical point. Clusters and loops that are otherwise exponentially suppressed can grow without bound when the Boltzmann factor becomes unity and, thus, gain configurational entropy without energy cost.

The picture of the transition in liquid ^4He in terms of proliferating vortices, which disorder the system and thereby restore the spontaneously broken $U(1)$ symmetry, has been advanced since then by various authors¹⁰. Early numerical evidence for this picture based on Monte Carlo simulations of the three-dimensional XY model was given in Refs. 11, 12, 13. Analytic methods to describe the transition using vortex loops were further developed by Williams¹⁴, and by Shenoy and collaborators¹⁵. More recent numerical work on the three-dimensional XY model from the perspective of vortices, in particular their loop size distribution, can be found in Refs. 16, 17, 18, 19.

The famous drawing (see Fig. 1) introduced by the psychologist J. Jastrow serves as a metaphor for the approach followed in these notes. The drawing of a three-dimensional snow version of which was sculptured by students attending the Kevo Winter School to guard Vortexland stands for superfluid phase transitions, which can be described either in the conventional (duck) way¹, or in the Onsager (rabbit) way pursued here.

The next section discusses cluster percolation the paradigm of geometrical phase transitions in its pure form known as uncorrelated percolation (Sec. II) and in its applied form known as correlated percolation to describe thermal phase transitions in spin models (Sec. IIB) and the liquid-gas transition (IIC). Section III gives a parallel treatment of random walks, in its pure form (IIIA) and in its applied form to describe random (IIIB) and correlated vortex tangles featuring in superfluid phase transitions (IIIC) and also in superfluid turbulence and defect formation after a rapid phase transition (IIID). The section is set up such as to highlight the close similarity between cluster percolation and loop proliferation. Section IV describes vortex lines in detail, starting with noninteracting vortices (IVA), followed by including interactions (IVB) and an external field (IVC). Section V discusses entangled vortex lines as they appear when the Abrikosov flux lattice melts (VA) from the perspective of Feynman's cooperative exchange ring theory of Bose-Einstein condensation (VB) and also discusses the order parameter describing this phase (VC).

II. CLUSTERS

In this section, the paradigm of geometrical phase transitions, viz. percolation, and its extension to describe thermal phase transitions are discussed.

A. Uncorrelated Percolation

To define (site) percolation, consider a lattice with N sites labeled by the index $1 \leq i \leq N$. Imagine visiting a site and generating a random number $0 < r_i < 1$. If that number is smaller than a pre-defined number p , the occupation probability, occupy the site, otherwise leave it unoccupied. This algorithm can be summarized in pseudo computer code as:

```
while i < N
```



FIG. 2: Typical output²⁰ of the site percolation algorithm implemented on a two-dimensional square lattice for $p < p_c$ (left panel) and $p = p_c$ (right panel). Occupied sites are marked by a dark square, with those belonging to the percolating cluster having a lighter grayscale, while unoccupied sites are unmarked.

```

generate  $0 < r_1 < 1$ 
if  $r_1 < p$  occupy site
i++
end while

```

After all lattice sites have been visited in this way, a random pattern of occupied and unoccupied sites emerges (see Fig. 2). Next-neighboring occupied sites can be grouped together into clusters, whose properties as a function of p form the subject of percolation theory. Since a given site is occupied whether or not neighboring (or any other) sites are, this process is more precisely referred to as uncorrelated percolation.

As the occupation probability p increases, more sites become occupied and the clusters grow. For high-enough values of p , a large cluster, spanning the lattice is frequently generated during updates (see the right panel of Fig. 2). The appearance of such a percolating cluster is a fundamental property and not an artifact of working on a finite lattice. Even on an infinite lattice, a percolating cluster, which would then be of infinite size, appears. The only difference between a finite and infinite lattice is that the percolating cluster on an infinite lattice first appears at a specific value p_c , special to the dimensionality and symmetry of the lattice considered, whereas on a finite lattice there is always a finite probability to generate a percolating cluster when $p < p_c$. Also, for $p > p_c$, the percolating cluster is always generated on an infinite lattice, but not necessarily so on a finite one. The theory of finite-size scaling is needed to extract the value of p_c from numerical simulations done on finite lattices²¹.

Percolation theory²² can be set up starting from the cluster size distribution $\nu_s(p)$, giving the number density of clusters of size s . Close to the percolation threshold, it takes the form

$$\nu_s(p) / s \sim e^{-cs}; \quad c / (p_c - p)^{1/\nu}; \quad (1)$$

where the coefficient c vanishes with an exponent $1/\nu$ when the percolation threshold p_c is approached from below. The cluster size distribution (1) contains two factors. The first one measures (as will become clear below when discussing random walks) the configurational entropy of clusters, while the exponential is similar to a Boltzmann factor which for finite c suppresses large clusters. The latter vanishes when the percolation threshold is approached from below, implying no longer a restriction on forming arbitrary large clusters and resulting in a proliferation of clusters.

Although percolation lacks a conventional description in terms of an Hamiltonian, a partition function Z can nevertheless be defined through

$$\ln(Z) / V = \sum_s \nu_s; \quad (2)$$

with V denoting the volume of the system. The right hand counts the number of clusters of all sizes. As in statistical physics, various physically relevant quantities can be calculated from Z , such as the percolation strength $P(p)$, which for $p > p_c$ denotes the probability that a randomly chosen site belongs to the percolating cluster, and the average cluster size $S(p)$. Specifically,

$$P = \frac{\partial \ln(Z)}{\partial c}; \quad S = \frac{\partial^2 \ln(Z)}{\partial c^2}; \quad (3)$$

showing that the percolation strength P is similar to the magnetization in spin models, while the average cluster size S is similar to the magnetic susceptibility. Near the percolation threshold, the quantities (3) show power-law

behavior, $P(p) \sim (p - p_c)^{-\nu_{\text{per}}}$ and $S(p) \sim |p_c - p|^{-\nu_{\text{per}}}$, characterized by the critical exponents ν_{per} and ν_{per} , where the subscript "per" is to indicate that they pertain to percolation. A final critical exponent, γ_{per} , specifies the power-law behavior of the correlation function G_{per} at the percolation threshold. Physically, $G_{\text{per}}(\mathbf{x}; \mathbf{x}^0)$ denotes the probability that the sites with position vectors \mathbf{x} and \mathbf{x}^0 belong to the same cluster. It usually is only a function of the distance between the two sites and has at $p = p_c$ the algebraic behavior in d space dimensions

$$G_{\text{per}}(\mathbf{x}) \sim \frac{1}{x^{d-2+\gamma_{\text{per}}}}; \quad (4)$$

The exponent γ_{per} , together with the so-called Fisher exponent²³, specifying the cluster size distribution (1), determine these critical exponents through scaling relations [see Eq. (10) below].

Since the percolating cluster, often also referred to as infinite cluster, includes a macroscopic fraction of the total number of sites, its mere size would dominate any sum. For this reason, summations \sum_s over cluster sizes exclude the percolating, or infinite one. In practice²¹, when working on a finite lattice, simply the largest cluster present is excluded, whether or not it spans the lattice. The percolation strength P can nevertheless be extracted from considering only finite clusters in Eq. (13) because of the constraint

$$p = P(p) + \sum_s s^{-1} S_s(p); \quad (5)$$

stating that an occupied site either belongs to the infinite cluster or to a finite one. This constraint is special to percolation.

Another important quantity characterizing percolation is the radius of gyration R_s ,

$$R_s^2 = \frac{1}{s} \sum_{i=1}^s (\mathbf{x}_i - \mathbf{x})^2; \quad (6)$$

which gives a measure of the spatial extent of a cluster of size s centered at $\mathbf{x} = (1/s) \sum_{i=1}^s \mathbf{x}_i$. For large enough clusters, R_s scales with s as

$$R_s \sim s^{1/D}; \quad (7)$$

defining the Hausdorff, or fractal dimension D . Close to the percolation threshold, D can be related to the correlation length exponent ν_{per} , specifying how the correlation length diverges, $(p - p_c)^{-\nu_{\text{per}}}$. The relation reads²²

$$\nu_{\text{per}} = \frac{1}{D}; \quad (8)$$

Also the Fisher exponent γ_{per} can be easily related to the fractal dimension, giving

$$\gamma_{\text{per}} = \frac{d}{D} + 1; \quad (9)$$

where d denotes the number of space dimensions.

Using scaling laws, one can express all the critical exponents in terms of just the two exponents ν_{per} and γ_{per} , specifying the cluster size distribution (1). For example²²,

$$\nu_{\text{per}} = \frac{2}{d-2D}; \quad \gamma_{\text{per}} = \frac{3}{d-2D}; \quad \nu_{\text{per}} = 2 + d - 2D; \quad (10)$$

with ν_{per} increasing from $36/91 \approx 0.40$ on a two-dimensional square lattice to $1/2$ on a six-dimensional square lattice, while at the same time, the fractal dimension increases from $D = 91/48 \approx 1.90$ to 4 . Six is the upper critical dimension of uncorrelated percolation, beyond which the exponents remain fixed at their mean-field values $\nu_{\text{per}} = 1/2$ and $D = 4$ ²².

The discussion so far concentrated on clusters of occupied sites, which for $p < p_c$ make up the minority phase, while the unoccupied sites form the majority phase. At the percolation threshold this changes and the roles of the minority and majority phases are interchanged. In other words, when approaching the percolation threshold from above, one would naturally concentrate on the disfavored unoccupied, rather than on the abundant occupied sites. From that side, the transition corresponds to a proliferation of clusters of unoccupied sites. In a sense, the two descriptions are dual to each other with the minority and majority phases interchanged.

B . Correlated Percolation

To see how percolation theory can be applied to therm alphase transitions taking place in spin models consider the Ising model at the absolute zero of temperature²². Here, in the absence of fluctuations, all the spins, which in principle can take the values $S_i = \pm 1$, point in one direction. When the temperature T increases, some of the spins will reverse their direction. The resulting spin configuration at a given temperature is easily mapped onto a percolation problem by identifying the sites with reversed spins with occupied sites. The question is now if the critical behavior of the Ising model can be recovered, focusing exclusively on these clusters instead of the magnetic properties. In other words, are the correct values for the critical temperature and the critical exponents obtained when measuring quantities like the percolation strength and the average cluster size discussed above?

It turns out that, in general, clusters of sites with reversed spins proliferate already before the therm alphase transition is reached. (Only on a two-dimensional square lattice, the temperature where a percolating cluster first appears coincides with the critical temperature.) Moreover, the critical exponents thus obtained are those of uncorrelated percolation and not of the Ising model (even on a two-dimensional square lattice). This means that the clusters constructed in this naive way lack essential information about the Ising model and need to be modified.

To construct a modified cluster²⁴, take two nearest-neighboring sites i, j of a naive cluster with its spins reversed, and include the pair into the modified cluster only with the bond probability

$$p_{ij} = 1 - \exp(-2J/k_B T); \quad (11)$$

where J is the spin-spin coupling of the Ising model and $\beta = 1/k_B T$, with k_B Boltzmann's constant. The factor $2J$ appearing here corresponds to the increase in energy when one of the two spins involved in the bond is flipped. The upshot of this modification is that the resulting bond clusters are in general smaller than the naive ones and also more loosely connected. The modified clusters turn out to proliferate right at the critical temperature and display critical behavior identical to that of the Ising model²⁵ as should be according to an exact map of the partition function of the Ising model onto correlated percolation by Fortuin and Kasteleyn²⁵.

The above scenario was recently extended to three-dimensional $O(n)$ spin models, with $n = 2; 3; 4$. Instead of taking only the two values $S_i = \pm 1$, which can be thought of as comprising a zero-dimensional sphere, the spins of the $O(n)$ model can take any value on the $(n-1)$ -dimensional sphere defined by $S_i^2 = 1$. The $O(n)$ model with $n = 2$ corresponds to the XY-model, while that with $n = 3$ corresponds to the Heisenberg model. An exact analytic map onto correlated percolation as existed for the Ising model is not available for $n > 1$, so that numerical simulations are needed to establish the existence of such a map²⁶. Two nearest-neighboring sites i and j with spin S_i and S_j are included in a cluster with bond probability

$$p_{ij} = 1 - \exp(-2J \max[0; (S_i - r) \cdot (S_j - r)]); \quad (12)$$

where r is a randomly chosen unit vector which can be used to cut the unit hypersphere $S_i^2 = 1$ in two halves (see Fig. 3). When the spins S_i and S_j take values in opposite halves of the hypersphere, their projections onto r have opposite sign. Such a pair is never included in a cluster since $p_{ij} = 0$ then. When the spins take values in the same half, the pair is included in a cluster with the bond probability determined by the projection $S_i \cdot r$ of their spin onto the random vector. The clusters thus constructed turn out to proliferate at the critical temperature where the therm alphase transition takes place. Moreover, the critical exponents obtained by measuring the percolation strength and average size of these clusters are the same as those obtained in the more traditional manner by focusing on the magnetic properties of these spin models²⁶.

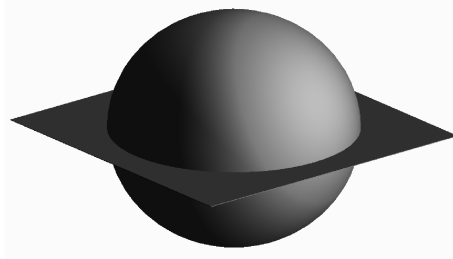


FIG. 3: A 2-sphere denoting the possible values a spin of the $O(3)$, or Heisenberg model can take. A randomly chosen vector r (not shown in the figure) can be used to cut the sphere in two halves, depending on the sign of the projections of a spin onto that vector.

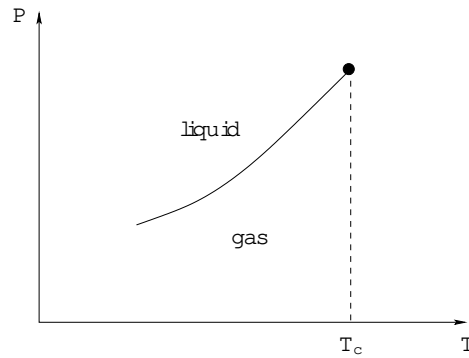


FIG. 4: Sketch of part of the liquid-gas phase diagram, showing the coexistence curve and the critical point at which this curve terminates.

These examples illustrate that thermodynamic phase transitions taking place in a wide range of statistical physics models can be reformulated in terms of percolation theory. Each of these models is thus characterized by a partition function of the form (2) with a cluster size distribution ψ_s given by Eq. (1). The exponents γ and β characterizing ψ_s take values specific for the universality class to which the model belongs. Given the values of γ and β , which in general differ from those of uncorrelated percolation, the critical exponents follow from scaling relations, as in Eqs. (8)–(10).

C. Liquid-Gas Transition

Next, the condensation of a classical gas, the liquid-gas transition, is considered from the perspective put forward by Mayer et al.^{27,28} and shown to be closely related to correlated percolation.

The relevant part of a typical phase diagram is sketched in Fig. 4. Below a critical temperature T_c , the gas phase is separated from the liquid phase by a discontinuous phase transition. At the phase boundary, the two phases have the same free energy and despite different particle number densities coexist, separated by an interface. The energy of the mixed state is higher than that of the pure states because the formation of the surface requires energy—the surface tension. The coexistence curve ends at a critical point where the surface tension vanishes and the transition becomes continuous with Ising model critical exponents. The order parameter, distinguishing the liquid from the gas phase, is the difference in particle number density.

In Mayer's theory, which was the first description of a phase transition beyond mean-field theory²⁹, the full interaction between molecules is approximated by a pair interaction. That is, three-particle and higher interactions, which are irrelevant when describing critical behavior, are ignored. The grand-canonical partition function $Z(\beta, \mu)$, with $\beta = 1/(k_B T)$, can then be written as an Ursell-Mayer cluster series^{27,30}

$$\ln(Z) = V \sum_{l=1}^{\infty} \frac{b_l}{l!} e^{\beta \mu l}; \quad (13)$$

where $b_l = \frac{1}{l!} \int d\mathbf{r}_1 \dots d\mathbf{r}_l \sum_{\text{clusters}} \dots$, with m the mass of a molecule, is the de Broglie thermal wavelength, and the b_l 's, with $b_1 = 1$, denote the Mayer cluster integrals²⁸. Being determined by the pair potential, these integrals can in principle be calculated, but, apart from small clusters, are in practice too complicated to evaluate for realistic choices of the potential. A (classical) ideal gas corresponds to setting $b_l = 0$ for $l > 1$. With the abbreviation

$$\gamma_l = \frac{b_l}{l!} e^{\beta \mu l}; \quad (14)$$

the partition function (13) can be written in a form similar to Eq. (2) for percolation,

$$\ln(Z) = V \sum_{l=1}^{\infty} \gamma_l; \quad (15)$$

while the expression for the number N of molecules, at least in the gas phase, becomes

$$N = \frac{\partial}{\partial \mu} \ln(Z) = V \sum_{l=1}^{\infty} l \gamma_l; \quad (16)$$

It is tempting to interpret ρ_1 as the number density of clusters containing l molecules. However, the Mayer cluster integrals b_l and therefore ρ_1 can be negative because the intermolecular interaction $u(r)$ is attractive for large separation r , behaving asymptotically as $u(r) \sim -1/r^6$. In the gas phase, where large clusters are exponentially suppressed so that only small clusters exist, the above interpretation is not obstructed too much³¹.

As for percolation, a possible infinite cluster, containing a macroscopic fraction of the total number N of molecules present, is excluded in summations ρ_1 over cluster sizes. (In numerical simulations, simply the largest cluster is best excluded, whether or not it spans the lattice.)

Condensation, achieved, say, by reducing the volume at fixed N , corresponds in this description to the formation of an infinite cluster. The sum $\sum_l l \rho_l$ in Eq. (16) denotes the number density of molecules in the gas phase, which is represented by the finite clusters. When the coexistence curve is reached at the volume V_{co} , the sum saturates at the value $N = V_{co}$. Upon reducing the volume further, an infinite cluster, which is not accounted for in the summation ρ_1 over cluster sizes, must form to accommodate the difference between the true density $N = V$ and that contained in the gas phase, $N = V_{co}$. For this to be possible, the exponential suppression of large clusters needs to vanish. Since the chemical potential remains negative at the coexistence curve, the Mayer cluster integrals must yield an l -dependent exponential factor to cancel the factor $\exp(-\beta \epsilon_l)$ in Eq. (14) at that curve. That is,

$$\frac{b_l}{3!} / l \sim e^{-\beta \epsilon_l}; \quad (17)$$

close to the coexistence curve, with the first factor measuring the configurational entropy of clusters³². It then follows that

$$\rho_1 / l \sim e^{-(\beta \epsilon_l)}; \quad (18)$$

so that as β approaches β_{co} from above, ρ_1 displays algebraic behavior, as required. This limit also marks the radius of convergence of the sum (16): for β smaller than β_{co} , the sum would diverge, i.e., at the coexistence curve³¹

$$\beta_{co} = \lim_{l \rightarrow \infty} (\ln l) / l; \quad (19)$$

The discontinuous liquid-gas transition fundamentally differs from the continuous phase transitions discussed so far. In the earlier discussion, the appearance of an infinite cluster signaled the (continuous) transition of the entire system from one phase into the other. That is, the infinite cluster together with the smaller clusters still present (see the right panel of Fig. 2) represent the new phase. In the liquid-gas transition, the situation differs in that the infinite cluster denotes the liquid phase, while the smaller clusters denote the gas phase. In other words, the right panel of Fig. 2 now represents a snapshot of a two-dimensional section of the system (in microgravity conditions, say) with both the liquid phase (percolating cluster) and the gas phase (smaller clusters) coexisting.

This interpretation is supported by the observation that the pressure associated with the infinite clusters satisfies the Clausius-Capeyron equation³¹. To first order, the pressure $P = -\ln(Z)/V$ in the gas phase can be approximated by that of an ideal gas, corresponding to the first term in the Ursell-Mayer expansion (13). When differentiated with respect to T , this gives

$$\frac{d \ln(P)}{dT} = \frac{1}{T} - \lim_{l \rightarrow \infty} \frac{1}{l} \frac{d \ln(b_l)}{dT}; \quad (20)$$

where use is made of Eq. (19). To interpret the last term, the energy $E = -d \ln(Z)/d\beta$ of the gas phase is determined, where β is to be considered a T -independent variable, leading to the result

$$E = V \sum_{l=1}^{\infty} l \rho_l; \quad (21)$$

with ϵ_l the energy per molecule of a cluster of size l ,

$$\epsilon_l = \frac{3}{2} k_B T + k_B T^2 \frac{1}{l} \frac{d \ln(b_l)}{dT}; \quad (22)$$

Since db_l/dT is in general negative, ϵ_l is smaller than the average kinetic energy per molecule, $\frac{3}{2} k_B T$. Physically, the last term in Eq. (22) denotes minus the (average) binding energy ϵ_l per molecule. In terms of this quantity, Eq. (20) becomes the Clausius-Capeyron equation³¹

$$\frac{d \ln(P)}{dT} = \frac{k_B T + \epsilon_1}{k_B T^2}; \quad (23)$$

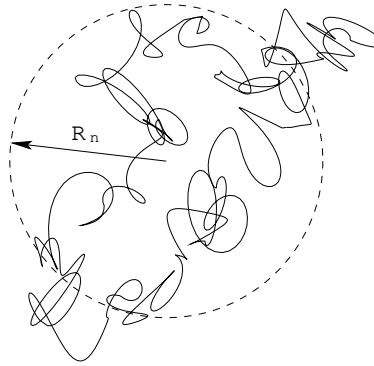


FIG. 5: Schematic representation of the radius of gyration R_n of a closed random walk containing n steps.

with the numerator at the right hand denoting the energy required to vaporize one molecule from the liquid, viz. the sum of the thermal energy $k_B T$ and binding energy ϵ_1 .

It should be kept in mind that the liquid-gas transition, being discontinuous, is special in that both the liquid and gas phase can coexist, each occupying separate parts of the total volume. Similar arguments as the ones developed for the liquid-gas transition are sometimes applied to an ideal Bose gas to argue that Bose-Einstein condensation is a discontinuous phase transition. A Bose-Einstein condensate is, however, formed in the zero-momentum state invading all of space and therefore intertwined with the non-condensed part. No interface separating the two parts exist. The situation is similar to that in the $O(n)$ spin models discussed above, where, at the critical temperature, the entire system transforms into a new phase that cannot be spatially resolved into two separate parts, each occupying its own volume.

Recently, the three-dimensional three-state Potts model in an external field has been numerically investigated, using clusters as fundamental objects³³. The phase diagram of this model is very similar to that of the liquid-gas transition, having a line of discontinuous phase transitions at small fields that terminates in a point at some critical field value where the transition becomes continuous with Ising model exponents.

III. RANDOM WALKS

The discussion of phase transitions so far was modeled after percolation theory, with clusters specified by the cluster size distribution (1) playing the central role. Another paradigm of thermal phase transitions is random walks to which the discussion now turns.

A. Brownian Random Walks

The simplest random walk is the Brownian random walk³⁴. On a d -dimensional square lattice, where each site has $2d$ nearest neighbors, a Brownian random walker located at a given site i randomly chooses among its nearest neighbors (n.n.) m_i the next site to visit. Here, the d unit vectors spanning the square lattice are denoted by \mathbf{j} . The random walker is not subject to any restriction and can, for example, return to a site it visited before. In pseudocode, the algorithm describing a Brownian random walk reads:

```
while i < n
  generate  $m_i$  f  $\mathbf{j}$ 
  move to n.n.  $m_i$ 
   $i++$ 
end while
```

A central concept in the theory of random walks is the probability $K_n(\mathbf{x} \rightarrow \mathbf{x}^0)$ for a random walker to move from one site with position vector \mathbf{x} to another \mathbf{x}^0 in n steps. The probability is given by

$$K_n(\mathbf{x} \rightarrow \mathbf{x}^0) = \frac{\# \text{ of paths } \mathbf{x} \rightarrow \mathbf{x}^0 \text{ in } n \text{ steps}}{\# \text{ of paths } \mathbf{x} \rightarrow ? \text{ in } n \text{ steps}}; \quad (24)$$

where the denominator, counting paths with arbitrary endpoints (indicated by ?), is included so that K_n is a genuine probability, taking values between 0 and 1. To evaluate it, imagine the random walker taking a first step to one of its nearest neighbors j . It then has only $n-1$ steps still available to reach the final destination x^0 , with probability $K_{n-1}(x + aj | x^0)$. That is, K_n satisfies the recurrence relation:

$$K_n(x | x^0) = \frac{1}{2d} \sum_j K_{n-1}(x + aj | x^0); \quad (25)$$

where the factor $2d$ denotes the number of nearest neighbors on a d -dimensional square lattice. When $K_{n-1}(x | x^0)$ is subtracted from both sides of Eq. (25), a difference equation is obtained

$$K_n(x | x^0) - K_{n-1}(x | x^0) = \frac{1}{2d} \sum_j [K_{n-1}(x + aj | x^0) - K_{n-1}(x | x^0)]; \quad (26)$$

with the obvious boundary condition $K_0(x | x^0) = \delta_{xx^0}$. The continuum limit is taken by simultaneously letting $a \rightarrow 0$ and $n \rightarrow \infty$, such that the length $L = na$ of the random walk satisfies $La = na^2 \rightarrow \text{const}$. The difference equation then turns into the differential equation

$$\nabla^2 K_n(x | x^0) = \frac{a^2}{2d} \nabla^2 K_n(x | x^0); \quad (27)$$

with the celebrated solution

$$K_n(x | x^0) = \frac{d}{2\pi a^2} \exp \left[-\frac{d}{2} \frac{(x - x^0)^2}{na^2} \right]; \quad (28)$$

where $na^2 \rightarrow \text{const}$. Each dimension the random walker is free to roam gives a contribution $\frac{1}{2\pi a^2}$ to the prefactor.

The radius of gyration R_n of a random walk containing n steps is defined by

$$R_n^2 = \frac{1}{n} \sum_{i=1}^n (x_i - x)^2; \quad (29)$$

As for clusters, it measures the spatial extent of the random walk containing n steps and centered at $x = (1/n) \sum_{i=1}^n x_i$ (see Fig. 5).

It scales with the number of steps as

$$R_n \sim n^{1/D}; \quad (30)$$

where for Brownian random walks, the fractal dimension is $D = 2$.

When the random walk is taken as representing a flexible polymer or vortex, the energy to create such a line object needs to be included. Let γ denote that energy per unit length, i.e., the line tension, then this is achieved by the modification

$$K_n(x | x^0) \rightarrow K_n(x | x^0) e^{-\gamma na}; \quad (31)$$

Because of the energy cost, the Boltzmann factor exponentially suppresses long lines, provided the line tension is positive. The total probability for a random walker to move from one site x to another x^0 using an arbitrary number of steps defines the correlation function $G(x; x^0)$, which is assumed to depend only on the distance between the two sites:

$$G(x; x^0) = \sum_n K_n(x | x^0) e^{-\gamma na}; \quad (32)$$

In the absence of external sources and boundaries, vortex lines cannot terminate inside the system and must form closed loops. The partition function describing a (grand canonical) ensemble of closed, noninteracting vortex lines is given by

$$\ln(Z) = V \sum_n \frac{1}{n} K_n(x | x) e^{-\gamma na}; \quad (33)$$

where the notation $K_n(x \rightarrow x)$ indicates that the random walk representing the vortex line starts and ends at the same point. The right hand of the equation is therefore x -independent, as required for a partition function. Since a closed loop of length na can be traversed starting from any of the n sites visited, the factor $1/n$ prevents overcounting. With the explicit solution (28), the partition function becomes

$$\ln(Z) = V \sum_n \frac{\gamma_n}{n}; \quad (34)$$

where

$$\gamma_n / n = e^{-na}; \quad = \frac{d}{D} + 1; \quad (35)$$

Physically, γ_n denotes the loop size distribution, giving the number density of loops containing n steps. In this way, the partition function is represented in a form surprisingly similar to that in percolation theory Eq. (2) and for the liquid-gas transition Eq. (15), with the proviso that not clusters, but loops are considered.

B. Random Vortex Tangles

Given the close similarity in describing uncorrelated clusters and random vortex loops, the question arises whether both systems are in the same universality class. To settle this question numerically, an algorithm similar to that for uncorrelated percolation is needed to generate a random vortex tangle, consisting of intertwined closed vortex loops. Such an algorithm is provided by the Vachaspati-Vilenkin algorithm³⁵ developed to study defect formation in rapid (cosmic) phase transitions³⁶.

Quantized vortex lines emerge when a $U(1)$ symmetry is spontaneously broken³. The vacuum of a state with such a broken symmetry is characterized by a phase factor $\exp(i\theta)$, with the phase θ changing by 2π when a vortex of unit topological charge is circled once.

Consider discretizing both space (to a three-dimensional square lattice, say, with N sites) and also the vacuum manifold, so that θ takes only certain discrete values in the interval $0 \leq \theta < 2\pi$. The restriction to this interval assures that only vortices of unit strength are generated. Imagine visiting a site of the lattice and randomly assigning it one of the discrete phase values. The random choice guarantees that phases at different lattice sites are uncorrelated. The Vachaspati-Vilenkin algorithm, with θ taking the minimum number three of different values, can be summarized in pseudocode as:

```
while i < N
```

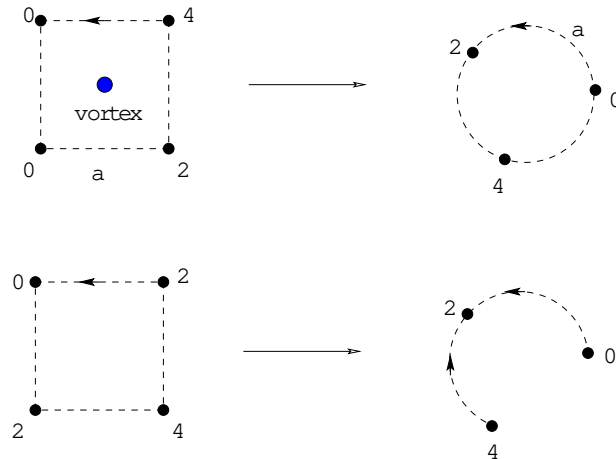


FIG. 6: Illustration of Kibble's geodesic rule³⁷. Top: Plaquette pierced by a vortex. The path segments labeled by a show the path taken by the phase along the vacuum manifold (circle at the right) when one moves from the left-lower to the right-lower corner on the plaquette circling the vortex. Bottom: Although all three available values of the phase appear, no vortex pierces the plaquette. When the right-lower corner is reached, where the phase is $4 \equiv 3$, the phase moves back to $2 \equiv 3$ rather than to 0 to complete the circle, representing the vacuum manifold.

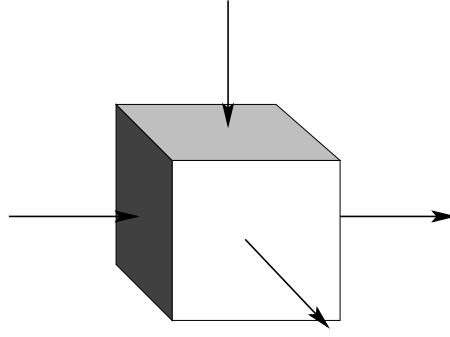


FIG. 7: Illustration of two vortices entering a (three-dimensional) unit cell.

```

generate  $\phi_i \in [0; \frac{2}{3}; \frac{4}{3}]$ 
i++
end while

```

After all lattice sites have been visited in this way, vortices are traced by going around each plaquette of the lattice once. When upon returning to the starting site, a phase difference of 2π is found, it is concluded that a vortex penetrates the plaquette. In going from one lattice site with the phase ϕ_1 to a neighboring site with the phase ϕ_2 , Kibble's geodesic rule³⁷ is used to select the shortest path along the circle representing the vacuum manifold connecting ϕ_1 and ϕ_2 (see Fig. 6 for two examples³⁵).

When two vortices are found to enter a unit cell (see Fig. 7), the two incoming and two outgoing vortex segments are randomly connected. After all the plaquettes of the lattice have been considered, a random vortex tangle, consisting of closed loops can be traced out.

The fractal dimension of the vortex tangle found in the initial simulations³⁵ were consistent with that of Brownian random walks, $D = 2$. This result can be understood⁷ by realizing that a dense random vortex tangle was simulated, where a single vortex experiences an effective repulsion from the neighboring vortex segments as the volume occupied by these segments is no longer available. This is similar to a polymer in a dense solution, which also executes a Brownian random walk.

In the Vachaspati-Vilenkin algorithm, the allowed phase values have equal probability so that the vortex tangle generated has always the same average vortex line density. To be able to vary the density, Vachaspati⁵ lifted the degeneracy of the vacuum manifold by giving one phase value a bias, $p_{2=3} = p_{4=3} \neq p_0$. This can be achieved by choosing for example⁷

$$p_{2=3} = p_{4=3} = C e^{-2}; p_0 = C e^{-1}; \quad (36)$$

with $C^{-1} = 2 \exp(-2) + \exp(-1)$. Since all phase values are needed for a vortex to pierce a given plaquette, the bias obstructs the formation of vortices and decreases the vortex line density. The bias parameter plays a role similar to that of the occupation probability p , determining the cluster density in percolation theory.

Imagine starting in the regime with only small vortex loops present and gradually changing the bias so that more and at the same time larger loops appear. It turns out that for small enough values of β an "infinite" vortex loop is frequently generated during updates⁵. The division between finite and infinite vortex loops is, of course, somewhat arbitrary on a finite lattice. A possible choice is to classify vortices with a length larger than³⁸

$$L_c = \frac{d}{2} \frac{L^2}{a} \quad (37)$$

as in finite, where L is the lattice size. The length scale L_c is the average length of Brownian random walks traversing the lattice once. In other words, most finite loops wrap themselves around the lattice and thus have a nonzero winding number. Universal quantities such as the critical exponents should be independent of the precise choice. On an infinite lattice, a threshold β_c exists, above which infinite vortex loops are absent and large, but finite loops exponentially suppressed. The sudden appearance of an infinite vortex loop as the threshold β_c is approached from above is similar to that of a percolating cluster in percolation theory⁵. For an infinite vortex to appear, the line tension needs to vanish, so that the Boltzmann factor in the loop size distribution (35) becomes unity and no longer suppresses large loops, i.e.,

$$\gamma_n(\beta) / n \rightarrow 0 \quad (38)$$

In analogy with percolation theory, cf. Eq. (1), the vanishing of the line tension is specified by an exponent ν ,

$$\sigma / (\sigma_c)^{1/\nu} : \quad (39)$$

At the threshold, vortex loops proliferate in the same way that clusters do at the percolation threshold.

To characterize the transition, the same definition of critical exponents can be used as in percolation theory, leading to the same scaling relations (10) found there. Numerical simulations of the transition that random vortex tangles undergo when changing the bias using this algorithm showed that the values for the critical exponents are more or less consistent with those of three-dimensional uncorrelated site percolation³⁹:

critical exponent	percolation theory	minimally discretized U (1)
	0.45	0.46(2)
ν_{per}	0.41	0.54(10)
ν_{per}	1.80	1.59(10)

Other values obtained in simulations with the discretized vacuum manifold given more than them in all three points³⁹, show even better agreement with percolation theory, implying that uncorrelated percolation and random vortex tangles are indeed in the same universality class. In other words, the close similarity in describing both phenomena discussed above extends to the level where fluctuations, determining the numerical values of the critical exponents, are included.

C. Correlated Vortex Tangles

In Sec. IIB, the extension of the theory of uncorrelated percolation to describe thermal phase transitions in correlated systems was discussed. It was concluded that correlated and uncorrelated percolation differ only in the specific values of the exponents ν and ν_{per} , specifying the cluster size distribution (1). The general framework applies to both cases, with the various expressions giving the critical exponents in terms of ν and ν_{per} remaining unchanged as they are protected by scaling laws.

Here, a similar extension is discussed for the random vortex tangle to describe superfluid phase transitions. An arbitrary—not just random—vortex tangle is again described by the loop size distribution (35)⁴⁰. In the superfluid phase, large vortex loops are exponentially suppressed. When the temperature increases, larger loops appear and the vortex tangle becomes denser. As the critical temperature is approached, the line tension σ vanishes, thereby allowing vortex loops to proliferate and thus to disorder the superfluid phase. The vanishing of the line tension is specified by the exponent ν ,

$$\sigma / (\sigma_c - T)^{1/\nu} : \quad (40)$$

As in correlated percolation, ν can be related to the fractal dimension D , introduced in (29), leading to the same relation (8). The value of the fractal dimension differs in general from the value obtained for a random vortex tangle or for Brownian random walks ($D = 2$). At criticality, the correlation function (32) shows algebraic behavior,

$$G(\mathbf{x}) \sim \frac{1}{x^{d-2+\nu}}; \quad (41)$$

as does the correlation function (4) defined in percolation theory. Using scaling laws, one can again express all the critical exponents in terms of the exponents ν and ν_{per} this time specifying the loop distribution.

However, with the exception of random vortex tangles discussed in the preceding subsection, usually not the percolation set of critical exponents, but a different set is used to describe vortex loops. The difference can be seen by considering the correlation function in percolation theory [above Eq. (4)] and for random walks [Eq. (32)], or more precisely their sum rules:

$$\sum_{\mathbf{x}} G_{\text{per}}(\mathbf{x}) / \sum_{\mathbf{s}} s^2 \nu_{\text{s}} / \sum_{\mathbf{s}} s^2 = e^{-c_{\text{s}}}; \quad (42)$$

and

$$\sum_{\mathbf{x}} G(\mathbf{x}) / \sum_{\mathbf{n}} n \nu_{\mathbf{n}} / \sum_{\mathbf{n}} n = e^{-c_{\text{n}}}; \quad (43)$$

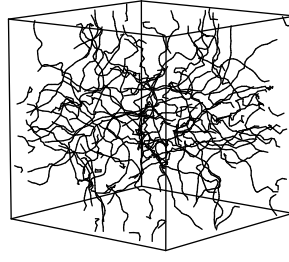


FIG. 8: Computed vortex tangle in pure superfluid turbulence without normal component. From Araki, Tsubota, and Nemirovskii⁴⁴.

respectively, where the sum \sum_x is over all lattice sites. The summands at the right sides of Eqs. (42) and (43) are seen to depend differently on the size (s and n , respectively). To understand the origin of this difference, note that the left sides equal the susceptibility for the respective order parameters. In general, χ is calculated from the partition function by differentiating it twice with respect to the conjugate field coupling linearly to the order parameter. The conjugate field is, for example, the magnetic field for magnetic systems, and the pressure for liquid-gas transitions. In other words, these correlation functions are tied to the definition of the order parameter, each having its own set of critical exponents.

For random walks, the set of critical exponents read in terms of the exponents ν and γ specifying the loop size distribution^{17,41,42}:

$$\nu_{ce} = \frac{2}{D}; \quad \gamma_{ce} = \frac{1}{D}; \quad \nu_{ce} = 2 - D : \quad (44)$$

Here, the critical exponent ν_{ce} , which specifies the vanishing of the order parameter when the critical temperature is approached, is given a subscript "ce" (for critical exponent) to distinguish it from the inverse temperature. These formulas should be compared to the analogous formulas in Eq. (10) for percolation. The expressions for ν_{per} and γ_{per} are directly related to the size-dependences in Eqs. (42) and (43). Brownian random walks, having fractal dimension $D = 2$, separate self-avoiding vortex loops ($D < 2$) from self-seeking ones ($D > 2$).

The two different sets of critical exponents, for percolation and for random walks, both satisfy the scaling laws. As only one correlation length features in both descriptions, cf. Ref. 43, the two sets have the exponent ν in common, implying that they are not independent. Consider, for example, the $O(2)$, or XY-model, whose thermal phase transition admits a description in terms of both correlated percolation and vortex loops. Let ν_{per} and γ_{per} specify the cluster size distribution discussed in Sec. IIB, and ν and γ the vortex loop size distribution (35), then

$$\frac{1}{\nu_{per} - 1} = \frac{1}{\nu}; \quad (45)$$

or written in terms of fractal dimensions,

$$\frac{D_{per}}{D} = \frac{1}{\nu}; \quad (46)$$

where D_{per} denotes the fractal dimension of the (bond) clusters, while D denotes that of the vortex loops at criticality.

D. Generating Vortex Tangles

The vortex tangles in superfluids discussed so far were generated by thermal fluctuations in the vicinity of the phase transition. At least two other ways to generate vortex tangles in superfluids are known.

(i) Consider setting up a counterflow, so that the superfluid and normal components move with different velocities, or dragging an object such as a grid through the superfluid. When a critical velocity is reached, the superfluid becomes turbulent through the formation of a random vortex tangle made up of quantized vortex loops⁴⁵ (see Fig. 8). For a constant, uniform counterflow, numerical simulations by Schwarz⁴⁶ showed that the vortex tangle can be self-sustained. In such counterflow turbulence, the normal component is possibly laminar and only the superfluid component turbulent. In superfluid grid turbulence, on the other hand, the superfluid and normal components are

believed to become locked together and behave like in classical turbulence, at least on scales where the quantization of vortices is irrelevant.

(ii) Consider heating a small region of the superfluid by, for example, radiating the cell with neutrons as in the Helsinki experiment on superfluid $^3\text{He-B}$ in rotation⁴⁸. When a neutron is absorbed by the superfluid, the energy deposited causes a small region to briefly heat up to the normal phase. After the subsequent rapid cool-down, a vortex tangle emerges. This scenario for defect formation after a rapid phase transition was first proposed by Kibble³⁷ in the context of cosmology and extended to condensed matter by Zurek⁴⁹. From the present perspective, the emergence of a vortex tangle after a rapid temperature quench is not so much the formation of defects, as well as the "freezing" into permanency of the dense vortex tangle rendering the hot bubble normal. In this sense, the vortex tangle emerging after the quench is a remnant of the normal phase. In addition to infinite loops, the normal phase has also many small vortex loops, which initially survive the rapid temperature quench. But as time passes, these small loops shrink to zero, leaving behind only larger ones traversing a macroscopic portion of the system (see Fig. 9). The larger loops by no means remain unchanged in time as they, through reconnections, spin off small loops, or hook up with other vortex loops to grow. The final configuration depends, of course, on the conditions under which the quench is performed, such as the presence of superflow. Apart from infinite vortex loops, which explains the expansion of the vortex tangle in Fig. 9, a superflow can also lead to additional mechanisms for defect formation, vortex loops wrapping around the bubble being created to screen the superflow from the interior⁴⁷.

IV. VORTEX ACTION

The discussion of vortex loops so far was qualitative as few details are needed to describe phase transitions in terms of vortex proliferation. In this section, a more detailed description of vortex lines is given.

A. Schrodinger Equation

To obtain the action describing vortex lines in a superfluid, the differential equation (27) satisfied by the transition probability $K_s(\mathbf{x} | \mathbf{x}^0)$ is written in the suggestive form

$$\partial_s K_s(\mathbf{x} | \mathbf{x}^0) = \frac{1}{2} \tilde{r}^2 K_s(\mathbf{x} | \mathbf{x}^0) \quad (47)$$

by introducing the arclength parameter s ,

$$s = \frac{a^2}{d} n \quad (48)$$

In this way, the differential equation becomes analogous to the time-dependent Schrodinger equation for the "time" evolution operator $K_s(\mathbf{x} | \mathbf{x}^0)$, satisfying

$$\partial_s \psi(\mathbf{x}; s) = -\frac{1}{2} \tilde{r}^2 \psi(\mathbf{x}; s) \quad (\mathbf{x}^0; 0); \quad (49)$$

where $\psi(\mathbf{x}; s)$ is the wave function at position \mathbf{x} and "time" s . The arclength parameter does not represent real time, but is the Schwinger proper time parameter⁵⁰. It parametrizes the path taken by the random walker, which is now

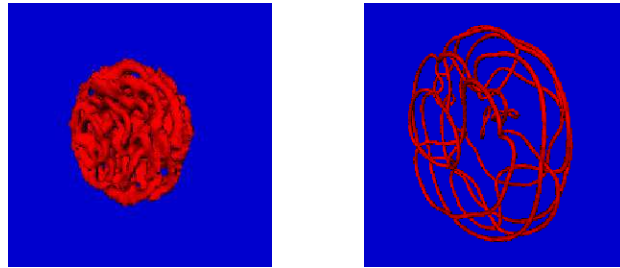


FIG. 9: Computed evolution of a vortex tangle in superfluid $^3\text{He-B}$ after a rapid temperature quench of a heated bubble in the presence of a superflow (perpendicular to the final configuration, resembling a snow chain). From Aranson, Kopnin, and Vinokur⁴⁷.

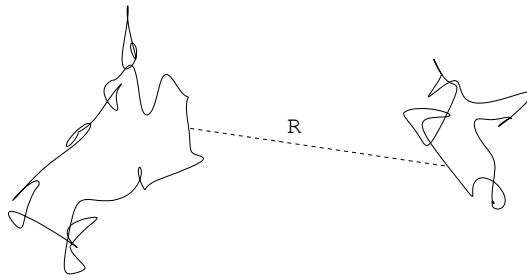


FIG. 10: Interaction between two line segments belonging to two different vortex loops.

pictured as a (bosonic) particle trajectory. The corresponding action reads:

$$S_0 = \sum_q \int ds \left[\frac{1}{2} \dot{x}_q^2(s) + \mu \right]; \quad \mu = d\tilde{\alpha}^2 = a; \quad (50)$$

where an extension to arbitrary many particles (labeled by q) is given, and the second term resulting from the modification (31) is included, with the vortex line tension. The action is given a subscript 0 to indicate that the interaction between vortex lines has been ignored for now. With one of the spatial coordinates interpreted as the time coordinate, the action (50) describes for $\tilde{\alpha} = 0$ the worldlines of relativistic particles of mass μ in d -dimensional spacetime⁵¹. The particles are at zero temperature, with the quantum fluctuations representing the thermal fluctuations of the vortex system at finite temperature.

To transcribe the (Euclidean) action (50), obtained using the quantum-mechanical analog into an Hamiltonian, the dimensionless combination $S/\tilde{\alpha}$ is to be replaced with H , so that the exponential factor $\exp(-S/\tilde{\alpha})$ becomes a Boltzmann factor:

$$\exp(-S/\tilde{\alpha}) \rightarrow \exp(-H); \quad (51)$$

The Planck constant $\tilde{\alpha}$ characterizing the quantum fluctuations of the equivalent zero-temperature particle system is replaced with the inverse temperature β characterizing the thermal fluctuations of the vortex system. The transcription is achieved by the change of variable

$$s \rightarrow s^0 = \frac{1}{2}\beta s; \quad (52)$$

where the factor $\frac{1}{2}$ is included for mere convenience. The transcribed action then reads

$$H_0 = \sum_q \int ds \left[\frac{1}{4} \dot{x}_q^2(s) + \frac{\mu}{L} \right]; \quad \frac{\mu}{L} = \frac{2d}{a}; \quad (53)$$

where the prime on the arclength parameter is suppressed, and the parameter L , which is determined by the vortex line tension μ , has the dimension of an energy per unit length. It follows from this expression that the line tension should scale linearly with a to obtain a finite value for the parameter L in the continuum limit. The correlation function (32) reads in these variables

$$G_0(\mathbf{x} - \mathbf{x}^0) = \frac{2d}{a^2} \int_0^1 ds K_s(\mathbf{x} - \mathbf{x}^0) = \frac{2d}{a^2} \int_0^1 ds \frac{1}{4s} \exp\left[-\frac{(\mathbf{x} - \mathbf{x}^0)^2}{4s}\right] e^{-\frac{\mu}{L}s}; \quad (54)$$

The exponent $d=2$ in the first factor of the integrand at the right hand expresses the fact that the random walker can roam in d dimensions, each giving a contribution $\frac{1}{4s}$.

B. Interaction

1. Superfluids

In this subsection, the interaction between vortex loops in a superfluid is considered. The pairwise interaction is mediated by the Goldstone mode associated with the spontaneously broken $U(1)$ symmetry. Being gapless, this mode

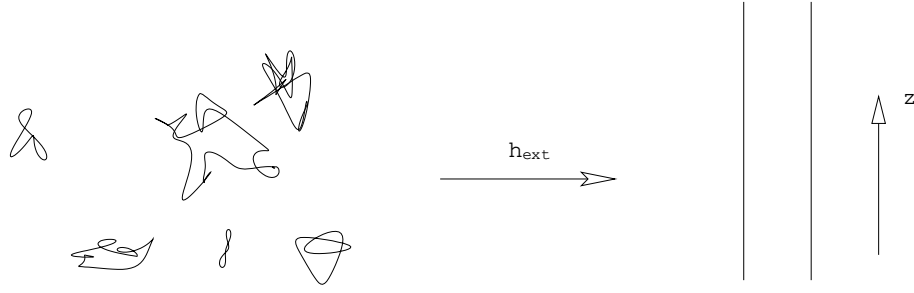


FIG. 11: Suppression of vortex loops and creation of open vortex lines when an external magnetic field is applied.

leads to a $1/R$ interaction in three space dimensions,

$$\frac{1}{R} = \frac{1}{(2\pi)^3} \int \frac{d^3k}{k^2} e^{ik \cdot R} \quad (55)$$

Each segment of a vortex line interacts via this potential with all other line segments of the same vortex as well as of the other vortices (see Fig. 10). The potential energy V of a vortex tangle is therefore of the form

$$V = \frac{1}{2} \frac{g^2}{4} \int_{q,q^0} \int ds \int ds^0 \frac{1}{R} \quad (56)$$

Here, g is the charge of a vortex given by

$$g^2 = \frac{h^2}{m^2} \quad (57)$$

with $h = m$ the circulation quantum and m the superfluid mass density, while R is the distance between two line segments, $R = |\mathbf{x}_q(s) - \mathbf{x}_{q^0}(s^0)|$. The mass parameter m denotes the mass of the atoms (for bosonic superfluids) or that of a pair of atoms (for fermionic superfluids). The integrations in Eq. (56) are along the vortex loops parameterized by their arclength parameters s and s^0 . Since V decreases with increasing R , the pair interaction between vortex segments with like-charges is repulsive. The total Hamiltonian H describing a vortex tangle consists of the sum of the free part (53) and the potential energy (56),

$$H = H_0 + V \quad (58)$$

For two slightly deformed rectilinear vortices parallel to the z axis, each of length L and separated by a distance $r(z)$, the right hand of Eq. (56) reduces to the well-known logarithmic form

$$V = \frac{g^2}{4} \int_0^L dz \int_0^L dz^0 \frac{1}{r^2(z) + z^2} = \frac{g^2}{4} \int_0^L dz \ln \frac{r(z)}{L} \quad (59)$$

The dependence on the vortex length L in the argument of the logarithm derives from the slow fall-off of the $1/R$ interaction.

2. Superconductors

The results obtained for superfluids are easily adapted for superconductors. The major difference is that the would-be Goldstone mode turns the long-ranged electromagnetic interaction into a screened one through the Higgs mechanism. This leads to the modification

$$\frac{1}{R} \rightarrow \frac{e^{-R/\lambda}}{R} \quad (60)$$

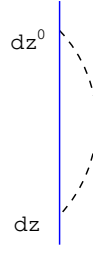


FIG. 12: Two line segments of the same vortex (solid line) interacting via the $1/R$ potential (dashed line).

in Eq. (56), where λ_L is the London penetration depth. The charge g of a magnetic vortex is again given by Eq. (57) for a superfluid, although it is usually put in the equivalent form

$$g = \frac{\phi_0}{2\pi}; \quad (61)$$

where ϕ_0 is the magnetic flux quantum. Note that g is independent of the electric charge e . The e -dependences in ϕ_0 and the penetration depth precisely cancel in the right hand of Eq. (61). Since the interaction is screened, the potential energy between two parallel slightly deformed rectilinear magnetic vortices separated by a distance $r(z)$ is

$$V = \frac{g^2}{4} \int_0^{Z_L} dz \int_0^{Z_L} dz^0 e^{-\frac{P}{r^2(z) + z^2}} = \frac{g^2}{4} \int_0^{Z_L} dz K_0 \left(\frac{r(z)}{\lambda_L} \right); \quad (62)$$

with K_0 a modified Bessel function of the second kind, which for small argument x behaves as $K_0(x) \sim -\ln(x)$. The role of infrared cutoff is now played by the London penetration depth λ_L .

C. External Field

From the present perspective, the major effect of turning on an external magnetic field is to suppress fluctuations along the field. In other words, the random walker representing the vortex trajectory is forced to move only in the direction of the applied field, and cannot move backwards (see Fig. 11). The external field thus suppresses the formation of vortex loops and (under certain conditions discussed below) instead leads to open vortices along the field direction, starting at the bottom of the sample and terminating at the top. The vortices can now only fluctuate around their equilibrium position by making excursions in the plane perpendicular to the field. In the quantum-mechanical analog, this corresponds to taking the nonrelativistic limit.

To study the effect of applying an external field, which is assumed to be parallel to the z axis, write

$$(x - x^0)^2 = r^2 + c^2 z^2; \quad (63)$$

where $r(z) = [x(z); y(z)]$ are the coordinates perpendicular to the field, parametrized by z . The parameter c is introduced (via the replacement $z \rightarrow cz$) to facilitate interpreting the spatial coordinate z as a time coordinate. The observation that fluctuations along the field are suppressed is implemented by letting $c \rightarrow 1$. In this limit, the integral over the Schwinger proper time parameter s in Eq. (54) can be approximated by the saddle point⁵²

$$s = \frac{c}{2\lambda_L} z; \quad (64)$$

connecting s to the timelike variable z , with the result in three dimensions

$$\frac{a^2}{2d} G_0(\mathbf{x} - \mathbf{x}^0) = \frac{1}{4} \frac{1}{z} e^{-\lambda_L(z + r^2/2z)}; \quad (65)$$

Here, the parameter c is scaled away again by the replacement $cz \rightarrow z$ thereby undoing the earlier replacement in Eq. (63). The exponent in the prefactor at the right hand is unity now instead of $3/2$ as it was in the absence of a field.

It indicates that after applying the magnetic field only the two directions perpendicular to the field are still available to the random walker to roam, each giving a contribution $\propto 1/z$. The Hamiltonian (53) becomes in this limit

$$H_0 = \sum_q \int_{-L/2}^{L/2} ds \left[\frac{1}{4} \dot{x}_q^2(s) + \frac{1}{2} \mu_L \right] + \sum_q \int_{-L/2}^{L/2} dz \left[\frac{1}{2} \mu_L \phi_q^2(z) + \mu_L \right]; \quad (66)$$

where use is made of Eq. (64). This procedure of taking the nonrelativistic limit is equivalent to the one used by Fetter⁵³ of expanding in small displacements in the xy plane. With z interpreted as the time coordinate, this Hamiltonian becomes, using the transcription (51), an action describing nonrelativistic bosons of mass μ_L moving in a plane in the presence of a constant background potential μ_L . As in the absence of an external field, the vortices, which are now open lines, are interpreted as the worldlines of particles, with the quantum fluctuations representing the thermal fluctuations of the vortex system. The limit taken in Eq. (66) precisely corresponds to the nonrelativistic limit of the relativistic Hamiltonian (53). The interaction between two "nonrelativistic" vortex lines is given by Eq. (62) as the case of slightly deformed rectilinear vortices considered there precisely describes vortices in the presence of an external field.

Not only two line segments belonging to different vortices interact via the $1/R$ potential, but also two line segments of the same vortex (see Fig. 12), giving the contribution to the energy

$$\frac{g^2}{4} \int_0^Z \int_0^Z dz^0 \frac{e^{-\mu_L \sqrt{(z-z^0)^2}}}{\sqrt{(z-z^0)^2}} = \frac{g^2}{4} \int_0^Z dz \ln \left(\frac{2}{\mu_L} \right); \quad (67)$$

where the coherence length ξ is taken as ultraviolet cutoff. This contribution amounts to a renormalization of the parameter μ_L . In the following, that parameter, introduced in Eq. (53), is assumed to be given by the integrand at the right hand of Eq. (67), representing the self-interaction energy per unit length, i.e.,

$$\mu_L = \frac{g^2}{4} \ln \left(\frac{2}{\mu_L} \right); \quad (68)$$

where $\mu_L = \mu_L$ is the Ginzburg-Landau parameter. The total Hamiltonian H describing vortices in the presence of an applied magnetic field is then given by the sum of the free part (66) and the interaction part

$$H_{\text{int}} = \frac{g^2}{4} \sum_{q \neq q^0} \int_{-L/2}^{L/2} dz \int_{-L/2}^{L/2} dz^0 \frac{[x_q(z) - x_{q^0}(z^0)]^2}{\sqrt{(z-z^0)^2}} + \sum_q \int_{-L/2}^{L/2} dz h_{\text{ext}}[x_q(z)]; \quad (69)$$

where the last term represents the interaction of the vortex lines with the external field. This field penetrates the sample only if the sum of the constant terms in Eqs. (66) and (69) becomes negative, i.e., when

$$h_{\text{ext}} > \frac{L}{\xi} = h_{c1}; \quad (70)$$

defining the lower critical field h_{c1} . Below this critical field, the system is in the Meissner state where the external field is excluded from the superconductor. Above h_{c1} , the system is in the mixed state where the external field invades the superconductor through an array of magnetic vortex lines. When fluctuations can be ignored, the repulsive pair interaction between the vortices makes them form a triangular Abrikosov flux lattice⁵⁴.

V. ENTANGLED VORTEX LINES

In this section, vortex tangles of a different kind than the ones above are discussed. Instead of consisting of closed vortex loops, the tangles considered here consist of open vortex lines, connecting the top and bottom of the sample due to an applied magnetic field (for superconductors) or rotation (for superfluids).

A. Vortex Lattice Melting

The equivalent particle system of nonrelativistic interacting bosons in 2+1 dimensions (with the z coordinate interpreted as a timelike variable) specified by the Hamiltonian $H = H_0 + H_{\text{int}}$ given in Eqs. (66) and (69) was taken by Nelson⁵⁵ as starting point to investigate the effect of thermal fluctuations on the Abrikosov vortex lattice. A similar approach to study fluctuations in vortex lattices in rotating ⁴He and in superconductors was pioneered



FIG. 13: Artist's impression of the Abrikosov vortex lattice (left panel) and the entangled vortex liquid (right panel). Periodic boundary conditions in the z direction are assumed.

by Fetter⁵³. In the particle system, the vortex lattice corresponds to a Wigner crystal resulting from the repulsive pairwise interaction between the particles. The thermal fluctuations of the vortex system translate into quantum fluctuations of the equivalent particle system, which, when violent enough, were predicted to melt the crystal. The resulting phase in the equivalent particle system is the superfluid phase⁵⁵, which is generally believed to be the sole alternative to the crystal phase for interacting bosons at low temperatures in a clean system without impurities. The superfluid phase corresponds to entangled vortex lines in the vortex system (see Fig. 13).

The importance of quantum fluctuations in a system of interacting bosons is measured by the so-called de Boer parameter⁵⁶. This dimensionless parameter can be obtained by writing the kinetic term at the right hand of Eq. (66) and the pair interaction term in Eq. (69) as

$$H^0 = \int d^3u \frac{1}{2} \sum_q \mathbf{r}_q^2(u) + \sum_{q < q^0} K_0 \frac{[\mathbf{r}_q(u) - \mathbf{r}_{q^0}(u)]^2}{2}; \quad (71)$$

where $u = ag^2z/2$ and

$$\frac{1}{2} = \frac{p}{a^2 g^2 L^2}; \quad (72)$$

with all length scales now being given in units of a typical length a , e.g., the lattice spacing when working on a lattice. The vortex lattice melting transition into an entangled vortex liquid was numerically shown to take place at the critical value $\mu_m = 0.062^{57}$. There is ample numerical⁵⁸ as well as experimental⁵⁹ evidence that the transition is discontinuous in a clean system. Further experimental results have been reported⁶⁰, indicating that the discontinuous melting line in the h - T phase diagram terminates at a critical point in the high-field, low-temperature corner.

B. Feynman's cooperative exchange rings

As was pointed out by Nelson⁵⁵, the entangled vortex liquid can be elegantly understood in the equivalent particle system, using Feynman's cooperative exchange ring theory of the transition in ^4He ⁶¹. Bose-Einstein condensation (BEC) is understood in this picture as follows. At finite temperature, the $(3+1)$ -dimensional ^4He particle trajectories form closed loops because the (Euclidean) time coordinate is compactified, taking values only in the interval $[0; \sim]$. For an ensemble of bosons, the boundary conditions are periodic, meaning that the configuration at time 0 and at time \sim are identical. In the normal phase, most bosons execute during this time interval a random walk in space (see left panel of Fig. 14), which starts and ends at the same position (indicated by a dot). It means that the particles, being distinguishable, behave classically. When the critical temperature is approached from above, the particles lose their identity and become indistinguishable. In Feynman's theory this is reflected by the formation of so-called cooperative exchange rings, where individual worldlines hook up to form larger loops⁶² (see right panel of Fig. 14). A particle in such a composite ring moves in imaginary time along a trajectory that does not end at its own starting position, but at that of another particle. Hence, although the initial and final configurations are identical, the particles in a composite ring are cyclically permuted.

To determine the condition for this to happen, consider an ideal Bose gas for simplicity. The non-interacting particles are described by a time evolution operator $K(x \rightarrow x^0)$, satisfying the time-dependent Schrödinger equation (47) with the Schwinger proper time parameter s introduced in Eq. (48) now replaced by the (Euclidean) time

$$s = \frac{a^2 m}{d} n; \quad (73)$$

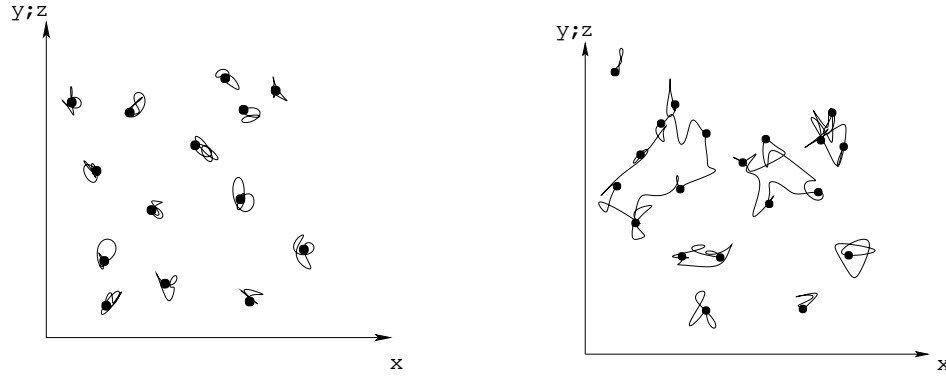


FIG. 14: Trajectories of non-interacting bosons in three space dimensions executed during the (imaginary) time interval $\sim \tau$. For ease of representation the y and z axes are lumped together. The starting points of the Brownian random walks are indicated by dots. In the normal phase (left panel), most random walks end at their own starting point, whereas in the Bose-Einstein condensed phase (right panel) large cooperative exchange rings are formed, with the trajectory of one particle ending at the starting point of another. In this way, particles in a ring are cyclically permuted after an imaginary time $\sim \tau$. (Adapted from Ref. 63.)

The right hand explicitly depends on the particle mass m . It follows that during the time interval $\tau = \hbar / (mc^2)$, the particles execute a Brownian random walk with an average length

$$L_{\sim} = \frac{d}{2} \frac{\hbar^2}{ma^2} \quad (74)$$

determined by the de Broglie thermal wavelength λ_{\sim} . If the length scale L_{\sim} becomes, upon reducing the temperature, on the order of the interparticle distance, individual worldlines can hook up to form large loops. The particles participating in the exchange rings become indistinguishable and the system Bose-Einstein condenses. When worked out, this condition gives an estimate of the critical temperature T_c .

A ring made up of the worldlines of w particles wraps around the imaginary time cylinder w times. BEC corresponds in this picture to the appearance of long loops, wrapping arbitrarily many times around the imaginary time cylinder⁶⁴. In other words, as for vortex loops before (see Sec. III), this transition corresponds to a proliferation of loops| not of vortex loops, but of worldline loops this time. BEC can therefore be described as a percolation process⁶⁵. The worldline loop size distribution⁶³

$$\rho_w / w \sim e^{-(\epsilon_c / T)^w}; \quad (75)$$

with $\epsilon_c = \hbar^2 / (2ma^2)$ and $\epsilon_c = dD + 1$, gives the density of rings containing w particles, or, equivalently, the density of loops wrapping around the imaginary time cylinder w times. The "line tension" ϵ_c of the worldlines is determined by the chemical potential μ [as was the Boltzmann factor in the cluster size distribution (14) in Mayer's theory of the liquid-gas transition] and vanishes when the critical temperature is approached from above [cf. Eq. (18)]. Specifically,

$$\epsilon_c / (\hbar^2 / (2ma^2))^{1/d} = \mu / (k_B T_c) \quad (76)$$

The worldline loop size distribution then changes from an exponential decay with increasing loop length to an algebraic decay. The winding number w in Eq. (75), denoting the number of particles contained in a ring plays the role of the number n of steps in the loop size distribution (35). In other words, a straight path segment traversed during a single step by a classical random walker now corresponds to a random trajectory traversed by a quantum particle during the time interval $\sim \tau$ [with an average length L_{\sim} given by Eq. (74) if the particle is non-interacting]. Since the loop size distribution is of statistical nature, details which require a resolution greater than the step size are irrelevant| whence the similarity in the loop distributions (75) and (35). Given the two exponents ϵ_c and $\epsilon_c^{1/d}$ specifying the worldline loop size distribution (75), the critical exponents characterizing the phase transition can again be obtained using scaling law s^{42} .

Feynman's picture of the transition is dual to the one based on vortex proliferation discussed earlier. Depending on whether the critical temperature is approached from below or above, vortices (in the superfluid phase), or worldlines (in the normal phase) proliferate. This is similar to the duality discussed in the context of percolation at the end of Sec. IIA, where clusters of the minority phase are considered in the sea made up of the majority phase: here either vortices in a sea of proliferated worldlines, or worldlines in a sea of proliferated vortices are considered.

Translated back to the vortex system, Fig. 14 represents the projections of the vortex lines onto a plane perpendicular to the applied field. The periodic boundary conditions of the equivalent particle system are somewhat unnatural for the vortex system, but are believed not to dramatically change the results, provided L , playing the role of \sim in the equivalent particle system, is large enough. The left panel of Fig. 14 mimics the Abrikosov flux lattice (apart from the lattice symmetry), with the vortex lines making only small excursions from the straight lines connecting the endpoints, while the right panel mimics the entangled vortex liquid. Precisely such snapshots of vortex positions were recently obtained in numerical simulations by Sen, Trivedi, and Ceperley⁵⁸.

C. Order Parameter of Entangled Vortex Liquid

A superfluid phase is characterized by the superfluid mass density ρ_s giving the response of the system to an externally imposed velocity \mathbf{v} . A computationally simple, yet powerful way of obtaining the superfluid mass density on a finite lattice with periodic boundary conditions was introduced by Pollock and Ceperley⁶⁶, who related ρ_s to the winding of particle trajectories around the lattice (not in the time direction, but in the space directions).

The free energy $F = -\frac{1}{\beta} \ln(Z)$ acquires an additional term after the boost

$$F_v = \frac{1}{2} V \rho_s v^2; \quad (77)$$

In the equivalent particle picture, this boost is implemented by letting

$$\frac{1}{2} m \dot{\mathbf{r}}_q^2 \rightarrow \frac{1}{2} m (\dot{\mathbf{r}}_q - \mathbf{v})^2 = \frac{1}{2} m \dot{\mathbf{r}}_q^2 - m \frac{d\mathbf{r}_q}{dt} \cdot \mathbf{v}; \quad (78)$$

leading to

$$e^{-F_v} = \int \prod_q d\mathbf{r}_q \exp \left[i \frac{m}{\hbar} \mathbf{w} \cdot \mathbf{v} \right]; \quad (79)$$

with the winding vector:

$$\mathbf{w} = \frac{1}{2\pi} \sum_q \oint_0^L d\mathbf{r}_q \left(\frac{d\mathbf{r}_q}{dt} \right); \quad (80)$$

To understand the appearance of the imaginary unit at the right hand of Eq. (79), note that in real time, particles are described by the phase factor $\exp(iS/\hbar)$. When going over to the Euclidean time variable τ , the term linear in the velocity retains the imaginary unit in the phase factor.

Since the integrand in the definition of the winding vector is a total derivative, only the endpoints of the integration contribute. In numerical simulations on a finite lattice, usually also periodic boundary conditions in the spatial directions are imposed. The winding vector then becomes

$$\mathbf{w} = \frac{1}{2\pi} \sum_q [\mathbf{r}_q(\sim L) - \mathbf{r}_q(0)] + L\mathbf{n}; \quad (81)$$

with L the linear size of space and \mathbf{n} a d -component vector with integer components, denoting the number of times the trajectories wrap around space in the x, y, \dots direction, respectively. Because of the periodic boundary condition in the τ direction, the sum in Eq. (81) is always zero, even when particles are cyclically permuted, so that a nonzero value for the winding vector obtains only when worldlines wrap around space, represented by the last term in Eq. (81). In the language used in connection with the length scale (37), such loops are classified as infinite. Expanding both sides of Eq. (79) to quadratic order in the applied velocity \mathbf{v} , one finds that⁶⁶

$$\langle \mathbf{w}^2 \rangle = dV g^2; \quad (82)$$

with g the vortex charge introduced in Eq. (57), $g^2 = (\hbar/m)^2 \rho_s$. It shows that the superfluid mass density is nonzero when infinite worldline loops are present. That is, ρ_s directly signals the proliferation of these loops and is therefore the proper order parameter describing the entangled vortex liquid.

The numerical simulations by Nordborg and Bletter⁵⁸ show that the superfluid mass density sharply rises at the critical value $\rho_m = 0.062$ from $\rho_s = 0$ in the crystal phase to ρ_s in the superfluid phase, where ρ_s is the total mass density.

VI. CONCLUSION

In these lecture notes, thermal phase transitions taking place in superfluids were discussed from a geometrical perspective. Two seemingly different geometrical approaches were treated: one modeled after cluster percolation and the other after loop proliferation first proposed by Onsager⁴. Apart from peculiarities resulting from differences in definition, the two geometrical approaches were, however, seen to be two faces of the same underlying formalism. Central in the description was the size distribution of clusters and loops, specified by two exponents from which in turn all the critical exponents characterizing the superfluid phase transition follow through scaling relations. At the critical point, two different types of clusters percolate and also two different types of loops proliferate, depending from which side the transition temperature is approached. The percolating cluster always belongs to the minority phase which then turns into the majority phase. The two percolation descriptions are dual to each other in that both phases are interchanged. Also the two loop descriptions are dual to each other, with finite vortex loops featuring in the superfluid phase and finite worldline loops featuring in the normal phase. These finite loops proliferate when approaching the critical temperature after which their roles are interchanged.

Finally, the similarity between the cluster distribution (18) and the worldline loop distribution (75), both depending on the fugacity $\exp(\dots)$, indicates that the descriptions in terms of clusters and worldline loops are in fact closely related. This connection is reinforced by the surprising presence of the de Broglie wavelength (which depends on \sim) in the classical partition function (13).

Acknowledgments

I'm indebted to M. K. Kuisi for the kind hospitality at the Low Temperature Laboratory in Helsinki and for inviting me to lecture at the Kevon Winter School, Kevon, Finland, 20-26 April 2002. I wish to thank H. A. Les for organizing and running the pleasant and inspiring Winter School; S. Balibar, R. Blaauwgeers, A. Fetter, R. Hanninen, N. Kopnin, M. K. Kuisi, L. Skrbek, E. Thuneberg, J. Viljas, and G. Volovik for fruitful discussions; T. Araki and N. Kopnin for allowance to reproduce their Fig. 8 and 9, respectively; and R. Blaauwgeers for Figs. 3 and 13.

This work was funded by the European Union program Improving Human Research Potential (ULTI III).

-
- ^y Electronic address: schakel@boojum.hut.
- ¹ See, for example, the contributions of A. L. Fetter (Bose-Einstein condensates), N. B. Kopnin (superconductors), and E. Thuneberg (superfluids) to this Kevon Winter School.
- ² S. Coleman, in: *New Phenomena in Subnuclear Physics*, edited by A. Zichichi (Plenum, New York, 1977).
- ³ P. W. Anderson, *Basic Notions of Condensed Matter Physics* (Benjamin-Cummings, New York, 1984).
- ⁴ L. Onsager, *Nuovo Cimento Suppl.* 6, 249 (1949); *Ann. NY Acad. Sci.* 51, 2867 (1949).
- ⁵ T. Vachaspati, *Phys. Rev. D* 44, 3723 (1991).
- ⁶ R. M. Bradley, P. N. Strensky, and J.-M. Debierre, *Phys. Rev. A* 45, 8513 (1992).
- ⁷ M. Hindmarsh and K. Strobl, *Nucl. Phys. B* 437, 471 (1995).
- ⁸ J. H. A. Kao, *Phys. Rev. E* 53, 6048 (1996).
- ⁹ R. P. Feynman, in: *Progress in Low Temperature Physics*, edited by C. J. Gorter (North-Holland, Amsterdam, 1955), Vol. 1, p. 17.
- ¹⁰ Early work can be found in: V. N. Popov, *Sov. Phys. JETP* 37, 341 (1973); F. W. Wiegand, *Physica (Utrecht)* 65, 321 (1973); *Introduction to Path-Integral Methods in Physics and Polymer Science* (World Scientific, Singapore, 1986); T. Banks, B. Meyer, and J. Kogut, *Nucl. Phys. B* 129, 493 (1977); R. Savit, *Phys. Rev. B* 17, 1340 (1978); *Rev. Mod. Phys.* 52, 453 (1980); W. Helfrich and W. Müller, in: *Continuum Models of Discrete Systems* (University of Waterloo Press, Waterloo, Ontario, Canada, 1980), p. 753; B. Halperin, in: *Physics of Defects, Proceedings of the 1980 Les Houches Summer School, Session XXXV*, edited by R. Balian, M. Klemm, and J.-P. Parier (North-Holland, Amsterdam, 1981).
- ¹¹ W. Janke, Ph.D. thesis, Freie Universität Berlin (1985).
- ¹² G. Köhler, R. E. Shrock, and P. W. Mills, *Phys. Rev. Lett.* 57, 1358 (1986).
- ¹³ H. Kleinert, *Gauge Fields in Condensed Matter* (World Scientific, Singapore, 1989).
- ¹⁴ G. A. Williams, *Phys. Rev. Lett.* 59, 1926 (1987); *ibid* 82, 1201 (1999).
- ¹⁵ S. R. Shenoy, *Phys. Rev. B* 40, 5056 (1989); B. Chattopadhyay, M. C. Mahato, and S. R. Shenoy, *Phys. Rev. B* 47, 15159 (1993).
- ¹⁶ N. D. Antunes and L. M. A. Bettencourt, *Phys. Rev. Lett.* 81, 3083 (1998).
- ¹⁷ A. K. Nguyen and A. Sudbø, *Phys. Rev. B* 60, 15307 (1999).
- ¹⁸ K. Kajantie, M. Laine, T. Neuhaus, A. Rajantie, and K. Rummukainen, *Phys. Lett. B* 482, 114 (2000).
- ¹⁹ P. O. Lönn, *Europhys. Lett.* 58, 705 (2002).

- ²⁰ These snapshots were generated using a Java applet by R. J. Gonsalves available at: www.physics.buffalo.edu/CompPhys_1998/Java/Percolation.html.
- ²¹ K. Binder and D. W. Heermann, *Monte Carlo Simulation in Statistical Physics: An Introduction* (Springer, Berlin, 1997).
- ²² D. Stauffer and A. Aharony, *Introduction to Percolation Theory* (Taylor & Francis, London, 1991).
- ²³ M. E. Fisher, *Physics* 3, 255 (1967).
- ²⁴ A. Coniglio and W. Klein, *J. Phys. A* 13, 2775 (1980).
- ²⁵ C. M. Fortuin and P. W. Kasteleyn, *Physica (Utrecht)* 57, 536 (1972).
- ²⁶ P. Blanchard, S. D'egal, S. Fortunato, D. Gandolfo, T. Mendes, and H. Satz, *J. Phys. A* 33, 8603 (2000).
- ²⁷ J. E. Mayer and S. F. Harrison, *J. Chem. Phys.* 6, 87 (1938).
- ²⁸ J. E. Mayer and M. Goeppert-Mayer, *Statistical Mechanics* (Wiley, New York, 1940).
- ²⁹ Interview of C. N. Yang conducted by K. Huang, www.networkchinese.com/chineseprof/interview.pdf: "Before 1938, in thermodynamics, there was this liquid phase, and there was another phase, which was the gas phase. Although made of the same molecules, they were rendered differently. Therefore the phases had nothing to do with each other. The liquid phase had its free energy, and the gas phase had its free energy, and when you match these free energies, or whatever, you get equilibrium | you get the phase transition. But in Mayer's work, he had only one partition function, and that partition function works both for the gas and the liquid. Ursell was before Mayer, but Ursell did not use his calculation to discuss phase transitions. I think if you check Mayer's papers, his ideas originated from many things Ursell did."
- ³⁰ H. D. Ursell, *Proc. Camb. Phil. Soc.* 29, 685 (1927).
- ³¹ R. Becker, *Theorie der Wärme* (Springer, Berlin, 1955).
- ³² Mayer took the Ansatz $b_l = B w^{l-1}$ with B and w two positive constants independent of l .
- ³³ S. Fortunato and H. Satz, *Nucl. Phys. B* 623, 493 (2002).
- ³⁴ H. Kleinert, *Path Integrals in Quantum Mechanics, Statistics and Polymer Physics* (World Scientific, Singapore, 1995).
- ³⁵ T. Vachaspati and A. Vilenkin, *Phys. Rev. D* 30, 2036 (1984).
- ³⁶ For a recent overview, see the various contributions in: *Topological Defects in Cosmology and Condensed Matter Physics*, edited by Yu. Bunkov and H. Godfrin (Kluwer, Dordrecht, 2000).
- ³⁷ T. W. B. Kibble, *J. Phys. A* 9, 1387 (1976).
- ³⁸ D. Austin, E. J. Copeland, and R. J. Rivers, *Phys. Rev. D* 49, 4089 (1994).
- ³⁹ K. Strobl and M. Hindmarsh, *Phys. Rev. E* 55, 1120 (1997).
- ⁴⁰ E. Copeland, D. Haws, S. Holbraad, and R. Rivers, in: *The Formation and Evolution of Cosmic Strings*, edited by G. W. Gibbons, S. W. Hawking, and T. Vachaspati (Cambridge University Press, Cambridge, 1990).
- ⁴¹ J. Hove, S. Mo, and A. Sudb, *Phys. Rev. Lett.* 85, 2368 (2000).
- ⁴² A. M. J. Schakel, *Phys. Rev. E* 63, 026115 (2001).
- ⁴³ A. Weinrib and S. Trugman, *Phys. Rev. B* 31, 2993 (1985).
- ⁴⁴ T. Arai, M. Tsubota, and S. K. Nemirovskii, in: *Proceedings of the International Symposium on Quantum Fluids and Solids, QFS 2001*, *J. Low Temp. Phys.* 126, 303 (2002); *cond-mat/0201405* (2002).
- ⁴⁵ See the various contributions in *Quantized Vortex Dynamics and Superfluid Turbulence*, edited by C. F. Barenghi, R. J. Donnelly, and W. F. Vinen (Springer, Berlin, 2001).
- ⁴⁶ K. W. Schwarz, *Phys. Rev. B* 38, 2398 (1988).
- ⁴⁷ I. S. Aranson, N. B. Kopnin, and V. M. Vinokur, *Phys. Rev. Lett.* 83, 2600 (1999).
- ⁴⁸ V. M. H. Ruutu, V. B. Eltsov, A. J. Gill, T. W. B. Kibble, M. Krusius, Y. G. Makhlin, B. Placais, G. E. Volovik, and W. Xu, *Nature*, 382, 334 (1996).
- ⁴⁹ W. H. Zurek, *Nature*, 317, 505 (1985).
- ⁵⁰ J. Schwinger, *Phys. Rev.* 82, 664 (1951).
- ⁵¹ R. P. Feynman, *Phys. Rev.* 80, 440 (1950).
- ⁵² C. R. Stephens, *Ann. Phys. (NY)* 181, 120 (1988).
- ⁵³ A. L. Fetter, *Phys. Rev.* 162, 143 (1967); *Phys. Rev.* 163, 390 (1967).
- ⁵⁴ A. A. Abrikosov, *Sov. Phys. JETP* 5, 1174 (1957).
- ⁵⁵ D. R. Nelson, *Phys. Rev. Lett.* 60, 1973 (1988); D. R. Nelson and S. Seung, *Phys. Rev. B* 39, 9153 (1989).
- ⁵⁶ J. de Boer, *Physica (Amsterdam)* 14, 139 (1948); in: *Progress in Low Temperature Physics*, Vol. 2, edited by C. J. Gorter (North-Holland, Amsterdam, 1957).
- ⁵⁷ W. R. M. Agno and D. M. Ceperley, *Phys. Rev. B* 48, 411 (1993).
- ⁵⁸ R. E. Hetzel, A. Sudb, and D. A. Huse, *Phys. Rev. Lett.* 69, 518 (1992); H. Nordborg and G. Blatter, *Phys. Rev. B* 58, 14 556 (1998); P. Sen, N. Trivedi, and D. M. Ceperley, *Phys. Rev. Lett.* 86, 4092 (2001), and references therein.
- ⁵⁹ H. Safar, P. L. Gammel, D. A. Huse, D. J. Bishop, J. P. Rice, and D. M. Ginsberg, *Phys. Rev. Lett.* 69, 824 (1992); E. Zeldov, D. Majer, M. Konczykowski, V. B. Geshkenbein, V. M. Vinokur, and H. Shtrikman, *Nature (London)* 375, 373 (1995); A. Schilling, R. A. Fisher, N. E. Phillips, U. Welp, D. Dasgupta, W. K. Kwok, and G. W. Crabtree, *ibid* 382, 791 (1996), and references therein.
- ⁶⁰ H. Safar, P. L. Gammel, D. A. Huse, D. J. Bishop, W. C. Lee, J. Giapintzakis, and D. M. Ginsberg, *Phys. Rev. Lett.* 70, 3800 (1993).
- ⁶¹ R. P. Feynman, *Phys. Rev.* 90, 1116 (1953); *ibid* 91, 1291 (1953); *Statistical Mechanics* (Benjamin, Reading, 1972).
- ⁶² D. M. Ceperley, *Rev. Mod. Phys.* 67, 279 (1995).
- ⁶³ S. Bund and A. M. J. Schakel, *Mod. Phys. Lett. B* 13, 349 (1999).
- ⁶⁴ M. Stone, *Int. J. Mod. Phys. B* 4, 1465 (1990).

⁶⁵ A . Sutō, J. Phys. A 26, 4689 (1993).

⁶⁶ E . L . Pollock and D . M . Ceperley, Phys. Rev. B 36, 8343 (1987).